

Article

Shape Phase Transitions in Even–Even $^{176–198}\text{Pt}$: Higher-Order Interactions in the Interacting Boson Model

Dongkang Li, Tao Wang and Feng Pan

Special Issue

Symmetry in Nuclear Physics: Model Calculations, Advances and Applications

Edited by

Prof. Dr. Jerry Paul Draayer, Dr. Feng Pan and Dr. Andriana Martinou



Article

Shape Phase Transitions in Even–Even $^{176–198}\text{Pt}$: Higher-Order Interactions in the Interacting Boson Model [†]

Dongkang Li ^{1,*}, Tao Wang ¹ and Feng Pan ^{2,*} ¹ College of Physics, Tonghua Normal University, Tonghua 134000, China² Department of Physics, Liaoning Normal University, Dalian 116029, China

* Correspondence: ldk667788@163.com (D.L.); daipan@dlut.edu.cn (F.P.)

† Dedicated to Jerry P. Draayer in celebration for his 80th birthday.

Abstract: Dynamical symmetry plays a dominant role in the interacting boson model in elucidating nuclear structure, for which group theoretical or algebraic techniques are powerful. In this work, the higher-order interactions required in describing triaxial deformation in the interacting boson model are introduced to improve the fitting results to low-lying level energies, $B(E2)$ values and electric quadrupole moments of even–even nuclei. As an example of the model application, the low-lying excitation spectra and the electromagnetic transitional properties of even–even $^{176–198}\text{Pt}$ are fitted and compared to the experimental data and the results of the consistent-Q formalism. It is shown that the results obtained from the model are better than those of the original consistent-Q formalism, indicating the importance of the higher-order interactions in describing the structure and the shape phase evolution of these nuclei.

Keywords: shape phase transition; higher-order interactions; the interacting boson model; Pt isotopes

Citation: Li, D.; Wang, T.; Pan, F. Shape Phase Transitions in Even–Even $^{176–198}\text{Pt}$: Higher-Order Interactions in the Interacting Boson Model. *Symmetry* **2021**, *14*, 2610. <https://doi.org/10.3390/sym14122610>

Academic Editor: Andrea Lavagno

Received: 9 November 2022

Accepted: 6 December 2022

Published: 9 December 2022

Publisher's Note: MDPI stays neutral with regard to jurisdictional claims in published maps and institutional affiliations.



Copyright: © 2020 by the authors. Licensee MDPI, Basel, Switzerland. This article is an open access article distributed under the terms and conditions of the Creative Commons Attribution (CC BY) license (<https://creativecommons.org/licenses/by/4.0/>).

1. Introduction

It has so far been shown that the interacting boson model (IBM) proposed by Arima and Iachello [1–5] is very successful in describing low-lying spectra of medium and heavy mass even–even nuclei [6,7]. Shape phase evolution in these nuclei has also been extensively investigated [8–11]. The dynamical symmetry concept plays a dominant role in the interacting boson model, for which group theoretical or algebraic techniques are powerful. The model with no distinction between neutrons and protons is called IBM-1, which is simply called IBM in this paper. In addition, as another application of symmetry concept in nuclear structure, it has been shown very recently that the charge and matter radii of $^{4,6,8}\text{He}$ and the sizes of the self-conjugate $A = 4n$ nuclei calculated from the quantitative geometrical thermodynamics in taking the symmetry of alpha-particle into account agree closely with observed values [12].

In the IBM, an even–even nucleus is treated as an inert closed-shell core plus valence nucleons or holes outside of the core. It is assumed that the valence-like nucleons are paired with angular momentum $l = 0$ or 2 , and can be approximately treated as s -bosons and d -bosons. Hence, the IBM is equivalent to the shell model confined within the neutron and proton valence shells truncated within S - and D -pair subspace [13] without Pauli exclusion. Since the total number of valence nucleons is a conserved quantity, the total number of bosons in the IBM is an invariant. The single s -boson and five d -boson creation operators denoted as $\{s^\dagger, d_\nu^\dagger\}$ ($\nu = -2, -1, \dots, 2$) form a basis of the vector representation of the $U(6)$ group [1,6]. Thus, the model Hamiltonian can be realized by 36 generators $\{s^\dagger d_\nu, d_\nu^\dagger s, d_\nu^\dagger d_{\nu'}, s^\dagger s\}$ of the $U(6)$ group after the second quantization procedure, and must be kept as an $SO(3)$ scalar due to the rotational symmetry of nuclei. As the consequence,

for the given total number of bosons N , all possible linearly independent N -boson states form the symmetric irreducible representation (irrep) $[N, 0]$ of the $U(6)$ group. Due to the $SO(3)$ invariance, the N -boson states organized as the basis vectors of the irrep $[N, 0]$ of $U(6)$ classified in a group chain $U(6) \supset SO(3)$ are convenient to be used in diagonalizing the model Hamiltonian.

In previous IBM descriptions of Pt isotopes, the model Hamiltonian only contains one- and two-body interactions [14,15]. However, electric quadrupole moments of low-lying states near the $O(6)$ limit are too small due to the $O(6)$ selection rules, which is obviously inconsistent to the experimental results. Besides the three- and four-body interactions required to describe triaxiality, an exponential modification to the strength of the quadrupole–quadrupole interaction has been proposed [16,17], which improves the fitting quality of low-lying excited states, $B(E2)$ values and electric quadrupole moments [17]. Based on the CQ Hamiltonian, we make use of the general quadrupole operators $Q_\nu(\chi)$ in replacing the $SU(3)$ generators $Q_\nu(-\sqrt{7}/2)$ in the rigid triaxial rotor descriptions [18,19] or the γ -soft rotor descriptions with the $O(6)$ generators $Q_\nu(0)$ [17] to construct a more general soft rotor model Hamiltonian, which is called the modified soft rotor model. The modified soft rotor model Hamiltonian includes the general quadrupole–quadrupole interaction, the three- and four-body terms, and the d -boson number operator. Hence, the model can be used to describe medium and heavy mass even–even nuclei with better fitting quality. As an example of the model application, some low-lying positive parity level energies, $B(E2)$ values and electric quadrupole moments of some low-lying states in the even–even $^{176–198}\text{Pt}$ are fitted and compared to the experimental data and the results of the consistent-Q formalism.

2. The CQ Formalism and Its Extension

The simplest IBM Hamiltonian contains only one- and two-body terms, with other possible higher-order terms neglected. The compact form, in which the quadrupole operators in both the Hamiltonian and the $E2$ operator are taken to be the same, is called consistent-Q (CQ) formalism [20,21]. In the CQ formalism, the model Hamiltonian is expressed as [15,22]

$$\hat{H}_{\text{CQ}} = c \left(\eta \hat{n}_d + \frac{\eta - 1}{4N} Q(\chi) \cdot Q(\chi) \right), \quad (1)$$

where N is the total boson number, c is the scaling parameter, $\hat{n}_d = \sum_\nu d_\nu^\dagger d_\nu$ and $Q_\nu(\chi) = s^\dagger \tilde{d}_\nu + d_\nu^\dagger s + \chi (d^\dagger \times \tilde{d})_\nu^{(2)}$ with $\tilde{d}_\nu = (-)^\nu d_{-\nu}$, which are the d -boson number operator and quadrupole operator, respectively, $(d^\dagger \times \tilde{d})_\nu^{(k)}$ stands for the tensor coupling, and the parameters $\eta \in [0, 1]$ and $\chi \in [-\frac{\sqrt{7}}{2}, \frac{\sqrt{7}}{2}]$. When the $SO(3)$ irreps characterized by the quantum numbers of the angular momentum of the bosons are embedded within the irrep $[N, 0]$ of $U(6)$, there are three and only three possible ways [6]:

$$\begin{array}{ccc} U(5) \supset O(5) \\ U(6) \supset O(6) \supset O(5) \supset SO(3), \\ \text{SU(3) or } \overline{\text{SU(3)}} \end{array} \quad (2)$$

where $U(5)$ is generated by $(d^\dagger \times \tilde{d})_\nu^{(k)}$ ($k = 0, 1 \dots, 4$), $O(6)$ is generated by $\{L_{\nu'} = \sqrt{10} (d^\dagger \times \tilde{d})_{\nu'}^{(1)}, (d^\dagger \times \tilde{d})_\mu^{(3)}, Q_\nu(0)\}$, in which $L_{\nu'} (\nu' = -1, 0, +1)$ are the total angular momentum operators of the bosons, $SU(3)$ is generated by $\{L_{\nu'}, Q_\nu(-\sqrt{7}/2)\}$, while $\overline{SU(3)}$ is generated by $\{L_{\nu'}, Q_\nu(+\sqrt{7}/2)\}$. It should be noted that $\overline{SU(3)}$ is isomorphic to $SU(3)$, but the generators of $SU(3)$ are obviously different from those of $\overline{SU(3)}$ with different geometric explanations shown in the following. When $\eta = 1$, the basis vectors of $U(6) \supset U(5) \supset O(5) \supset SO(3)$ are eigenstates of the Hamiltonian (1), which is called the $U(5)$ (spherical) vibrational limit of the model. In the $U(5)$ limit, the nuclear shape is spherical with small β -vibration. When $\eta = 0$ and $\chi = 0$, the eigenstates of the Hamiltonian (1) are

the basis vectors of $U(6) \supset O(6) \supset O(5) \supset SO(3)$, which is called the $O(6)$ (γ -unstable) limit. In the $O(6)$ limit, the nuclear shape is an ellipsoid with indefinite (unstable) triaxiality, where the triaxiality $0^\circ \leq \gamma \leq 60^\circ$ and the dimensionless quadrupole deformation parameter β are the Bohr variables to describe the shape of an ellipsoid used in the collective model [23]. When $\eta = 0$ and $\chi = \mp\sqrt{7}/2$, the eigenstates of the Hamiltonian (1) are the basis vectors of $U(6) \supset SU(3) \supset SO(3)$ with the minus sign or $U(6) \supset \overline{SU(3)} \supset SO(3)$ with the plus sign. The former is called the $SU(3)$ limit, in which the nuclear shape is an axially deformed prolate ellipsoid with $\gamma = 0^\circ$, while the latter is called the $\overline{SU(3)}$ limit, in which the nuclear shape is an axially deformed oblate ellipsoid with $\gamma = 60^\circ$. In the three limiting cases, the Hamiltonian (1) is invariant under the $U(5)$, $O(6)$, $SU(3)$ [$\overline{SU(3)}$] transformation, respectively. Therefore, $U(5)$, $O(6)$, and $SU(3)$ ($\overline{SU(3)}$) are the dynamical symmetry groups in the three limiting cases, respectively. Accordingly, within the CQ formalism, the shape of a nucleus is determined by the parameters (η, χ) , which can be represented vividly by the extended Casten triangle [8,9] shown in Figure 1, where the three vertices are labeled by the three limits of the CQ Hamiltonian, the $U(5)$ – $SU(3)$ and $U(5)$ – $\overline{SU(3)}$ sides are the connection of the $(\eta = 1, \chi = \mp\sqrt{7}/2)$ and $(\eta = 0, \chi = \mp\sqrt{7}/2)$ vertices, while the $SU(3)$ – $SU(3)$ side is the connection of the $(\eta = 0, \chi = -\sqrt{7}/2)$ and $(\eta = 0, \chi = \sqrt{7}/2)$ vertices, and the $O(6)$ point with $(\eta = 0, \chi = 0)$ is on the $SU(3)$ – $SU(3)$ side. The above correspondence between the special IBM parameters and the shape defined by the Bohr variables (β, γ) in the collective model was established by using the coherent state formalism [24–26]. By using the coherent state formalism, it is further shown that, besides the limiting cases, the point at $(\eta = 0.5, \chi = 0)$ along the $U(5)$ – $O(6)$ line shown in Figure 1 is the critical point of the $U(5)$ (spherical) to the $O(6)$ (γ -unstable) shape phase transition in the large- N limit, which is called the $E(5)$ dynamical symmetry in the collective model [27]. Similarly, the point at $(\eta = 0.4707, \chi = \mp\sqrt{7}/2)$ on the $U(5)$ – $SU(3)$ [$\overline{SU(3)}$] side is the critical point of the $U(5)$ (spherical) to the $SU(3)$ [$\overline{SU(3)}$] (axially deformed) shape phase transition in the large- N limit, which is called the $X(5)$ [$\overline{X(5)}$] dynamical symmetry in the collective model [28]. Anyway, the extended Casten triangle elucidates possible nuclear shapes and their evolutions with the variation of the model parameters η and χ in the CQ formalism, except that the triaxial shapes are missing.

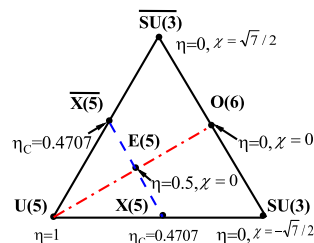


Figure 1. The extended Casten triangle in representing the entire parameter range of the IBM CQ formalism with the correspondence of the special model parameter values to the limits and the critical points of the shape phase transitions.

Since the IBM Hamiltonian with up to two-body interactions is unable to describe stable triaxial deformation, in order to reproduce a γ -rigid triaxial shape, higher-order terms have to be included [29–35]. For example, the IBM Hamiltonian with $[[d^\dagger \times d^\dagger]^{(k)} \times d^\dagger]^{(3)} \cdot [[\tilde{d} \times \tilde{d}]^{(k')} \times \tilde{d}]^{(3)}$ term can give rise of the stable triaxial deformation [30]. It is shown that the double γ anharmonic vibration reflects the importance of three-body interaction [31]. A similar conclusion was also made in [32,33]. Moreover, the $O(6)$ symmetry-conserving higher-order interactions were investigated [34]. The influences of symmetry-conservation higher-order interactions in the β - and γ -band of the IBM $SU(3)$ limit were also discussed in detail [35], where the β -band refers to the excited levels following the rotational level pattern established on the first excited 0^+ level, and γ -band refers to those established on the second excited 2^+ level in the collective model, in which the β -band head (the first

excited 0^+ level) is due to the β -vibration excitation, while the γ -band head (the second excited 2^+ level) is due to the excitation related to the γ -vibration energy. In this case, the even-even nucleus concerned is assumed to be axially deformed with small β - and γ -vibrations. The situation in the transitional nuclei is different because the nuclear shape in this case is not prolate and often γ -unstable. Therefore, levels established on the second excited 2^+ level in transitional nuclei are often called quasi γ -band. In addition, it is shown that the rotational spectra, which is the result of the two-body SU(3) quadrupole–quadrupole interaction, can also be generated by using the triple coupling scalar of the O(6) quadrupole operator [36]. Although the two descriptions can offer similar rotational spectra, the electromagnetic transitional properties are quite different [37]. The model with the triple coupling scalar of the O(6) quadrupole operators was also used to describe the triaxial deformation and the prolate to oblate shape phase evolution [38].

In the IBM, the SU(3) implementation of a rigid triaxial rotor was established [18,19] based on the early observation [39,40]. Specifically, a general rotor Hamiltonian is given as

$$H_{\text{rot}} = A_1 L_1^2 + A_2 L_2^2 + A_3 L_3^2, \quad (3)$$

where L_α is the projection of the angular momentum onto the α -th body-fixed principal axis, and A_α is the corresponding inertia parameter, which can be expressed in terms of the Bohr variables (β, γ) in the collective model [23]. The asymmetry parameter κ related to the inertia ellipsoid is defined by

$$\kappa = (2A_1 - A_2 - A_3)/(A_3 - A_2). \quad (4)$$

The rotor is prolate when $A_1 = A_2 < A_3$ with $\kappa = -1$; oblate when $A_2 < A_1 = A_3$ with $\kappa = +1$; and most asymmetric when $A_1 = \frac{1}{2}(A_2 + A_3)$ with $\kappa = 0$ [39,40]. It is obvious that the shape referred to here is the dynamical shape determined by the inertia parameters along the principal axes, though it coincides with the geometric shape of the rotor in most cases. The algebraic image of the general rotor Hamiltonian (3) can be realized [39,40] by rewriting H_{rot} in a frame-independent form by introducing and using the angular momentum L_u and the mass quadrupole tensor operators \mathcal{Q}_u with

$$\begin{aligned} L_u &= \int \rho(\vec{r})(\vec{r} \times \vec{v})_u \, d\tau, \\ \mathcal{Q}_v &= \sqrt{16\pi/5} \int \rho(\vec{r})r^2 Y_{2v}(\Omega) \, d\tau, \end{aligned} \quad (5)$$

where $\rho(\vec{r})$ is the nuclear mass density, and the integration is over the whole nuclear volume. It can be proven that these operators satisfy the following commutation relations:

$$\begin{aligned} [L_u, L_v] &= -\sqrt{2}\langle 1u, 1v | 1u + v \rangle L_{u+v}, \\ [L_u, \mathcal{Q}_v] &= -\sqrt{6}\langle 1u, 2v | 2u + v \rangle \mathcal{Q}_{u+v}, \\ [\mathcal{Q}_v, \mathcal{Q}_v] &= 0, \end{aligned} \quad (6)$$

which thus generate the dynamical symmetry group of the quantum rotor, the semidirect product group $T_5 \otimes_s \text{SO}(3)$. In the body-fixed principal-axial system, one has [39,40]

$$\begin{aligned} L^2 &= L_1^2 + L_2^2 + L_3^2, \\ X_3 &= \sum_{\alpha\beta} L_\alpha \mathcal{Q}_{\alpha\beta} L_\beta = \lambda_1 L_1^2 + \lambda_2 L_2^2 + \lambda_3 L_3^2, \\ X_4 &= \sum_{\alpha\beta\gamma} L_\alpha \mathcal{Q}_{\alpha\beta} \mathcal{Q}_{\beta\gamma} L_\gamma = \lambda_1^2 L_1^2 + \lambda_2^2 L_2^2 + \lambda_3^2 L_3^2, \end{aligned} \quad (7)$$

where L_α and $\mathcal{Q}_{\alpha\beta}$ are the Cartesian form of L_u and \mathcal{Q}_u introduced in (5), and λ_α are the eigenvalues of \mathcal{Q} in the body-fixed principal-axial system: $\langle \mathcal{Q}_{\alpha\beta} \rangle = \lambda_\alpha \delta_{\alpha\beta}$. From (7), we have

$$L_\alpha^2 = [(\lambda_1\lambda_2\lambda_3)L^2 + \lambda_\alpha^2 X_3^c + \lambda_\alpha X_4^c]/(2\lambda_\alpha^3 + \lambda_1\lambda_2\lambda_3). \quad (8)$$

Thus, the rotor Hamiltonian (3) can be expressed as [39,40]

$$H_{\text{rot}} = aL^2 + bX_3 + b'X_4, \quad (9)$$

where the parameters a , b , and b' depend on the inertia parameters A_α and the eigenvalues of \mathcal{Q} with

$$\begin{aligned} a &= \sum_\alpha z_\alpha A_\alpha, & z_\alpha &= \lambda_1\lambda_2\lambda_3/D_\alpha, \\ b &= \sum_\alpha b_\alpha A_\alpha, & b_\alpha &= \lambda_\alpha^2/D_\alpha, \\ b' &= \sum_\alpha c_\alpha A_\alpha, & c_\alpha &= \lambda_\alpha/D_\alpha, \end{aligned} \quad (10)$$

and

$$D_\alpha = 2\lambda_\alpha^3 + \lambda_1\lambda_2\lambda_3. \quad (11)$$

The expression (9) was used to make the SU(3) realization of the rotor Hamiltonian in the IBM framework [18,19]. In the SU(3) realization [18,19], the mass quadrupole tensor components \mathcal{Q}_ν is replaced by the SU(3) generators $Q_\nu(-\sqrt{7}/2)$. Hence, besides the L^2 term, the high order terms

$$\begin{aligned} X_3 &= (L \times Q(-\sqrt{7}/2) \times L)^{(0)}, \\ X_4 &= \left((L \times Q(-\sqrt{7}/2))^{(1)} \times (L \times Q(-\sqrt{7}/2))^{(1)} \right)^{(0)} \end{aligned} \quad (12)$$

should be included in the Hamiltonian to describe a rigid rotor with fixed triaxiality [18,19,39]. Recently, it has been further shown that the IBM with the SU(3) third-order term can be used to describe the oblate shape [41] and to explain the $B(E2)$ anomaly in some neutron deficient nuclei [42–44]. It should be pointed out that the inertia parameters along the principal axes are indefinite due to the fact that γ is a variable in the O(6) limit, which answers why it is called γ -unstable, while the inertia parameters along the three principal axes are fixed when the rotor is realized in the SU(3) limit with nonzero b and b' in (9) corresponding to the rigid triaxial (γ -rigid) case.

Since the triaxiality of the rotor is always fixed when X_3 and X_4 are realized by using the SU(3) generators $Q_\nu(-\sqrt{7}/2)$ [19] or γ -indefinite (unstable) when the O(6) generators $Q_\nu(0)$ are used in X_3 and X_4 , in order to describe a more general situation of triaxial nuclei, we use the general quadrupole operators $Q_\nu(\chi)$ with $\chi \in [-\sqrt{7}/2, \sqrt{7}/2]$ to construct the high order terms X_3 and X_4 , with which the model is called modified soft rotor. The modified soft rotor model covers not only the rigid triaxial case with $\chi = \mp\sqrt{7}/2$ and the γ -indefinite (unstable) case with $\chi = 0$, but also the intermediate (soft) case with $\chi \in (-\sqrt{7}/2, 0) \cup (0, \sqrt{7}/2)$.

3. The Modified Soft Rotor Model

Based on the CQ Hamiltonian, in addition to the d -boson number operator and quadrupole–quadrupole interaction, the three- and four-body terms are introduced to cover the emergence of triaxiality. Thus, the modified soft rotor model Hamiltonian is expressed as

$$\begin{aligned} \hat{H} = & c_0 \left(\eta \hat{n}_d + \frac{\eta-1}{4N} e^{\xi Q \cdot Q} Q(\chi) \cdot Q(\chi) + \frac{2a_1}{N^2} (\hat{L} \times Q(\chi) \times \hat{L})^{(0)} \right. \\ & \left. + \frac{4a_2}{N^3} ((\hat{L} \times Q(\chi))^{(1)} \times (\hat{L} \times Q(\chi))^{(1)})^{(0)} + \frac{a_3}{4N} \hat{L} \cdot \hat{L} \right), \end{aligned} \quad (13)$$

where ξ, a_1, a_2, a_3 are the dimensionless real parameters, and $Q_\nu \equiv Q_\nu(-\sqrt{7}/2)$ in the exponential of the second term is adopted, which is introduced to reduce the excitation energies of the eigenstates with higher angular momentum, while the other terms are the same as those shown in (1). The microscopic shell model foundation of these high-order interactions is shown in [16]. Most importantly, instead of $Q_\nu(-\frac{\sqrt{7}}{2})$ for the rigid rotor in the SU(3) limit or $Q_\nu(0)$ of the γ -unstable rotor in the O(6) limit, the general quadrupole operators $Q_\nu(\chi)$ with $\chi \in [-\frac{\sqrt{7}}{2}, \frac{\sqrt{7}}{2}]$ are used in the three- and four-body terms. The Hamiltonian (13) not only maintains the consistency to the CQ Hamiltonian, but also covers the emergence of triaxiality, so it should provide a better description of structural evolution of medium and heavy mass nuclei.

It should be noted that the full set of the basis vectors of any group chain shown in (2) is complete. The Hamiltonian (13) is diagonalized in the $U(6) \supset SU(3) \supset SO(3) \supset SO(2)$ basis, of which the basis vectors are denoted as $\{|N(\lambda\mu)\kappa, LM\rangle\}$, where (λ, μ) labels the irreducible representation of the SU(3) group, κ is the additional quantum number required in the reduction $SU(3) \downarrow SO(3)$, L is the quantum number of the angular momentum, and M is the quantum number of the angular momentum projection. Thus, the eigenstates of the Hamiltonian (13) can be expressed as

$$|NL_\zeta\rangle = \sum_{(\lambda\mu)\kappa} C_{(\lambda\mu)\kappa}^{L_\zeta} |N(\lambda\mu)\kappa L\rangle, \quad (14)$$

where ζ labels different eigenstates, but with the same L , and $C_{(\lambda\mu)\kappa}^{L_\zeta}$ is the expansion coefficient. As with the CQ formalism, the E2 transition operators is defined as

$$T_\nu(E2) = q_2 Q_\nu(\chi), \quad (15)$$

where q_2 is the effective boson charge-related parameter. Hence, the $B(E2)$ values are given by

$$B(E2; L_\zeta \rightarrow L'_{\zeta'}) = \frac{1}{2L+1} |\langle NL'_{\zeta'} | T(E2) | NL_\zeta \rangle|^2, \quad (16)$$

in which the reduced matrix element $\langle NL'_{\zeta'} | T(E2) | NL_\zeta \rangle$ is defined in terms of the $3j$ -symbol according to the Wigner–Eckart theorem. A Fortan code of this work is written based on the results shown in [15,45], in which the $SU(3) \supset SO(3)$ Wigner coefficients are taken from the Draayer–Akiyama code [46].

4. Shape Phase Transition in $^{176-198}\text{Pt}$

Shape phase transition and possible cross-shell excitations in even–even Pt isotopes with mass number $172 \leq A \leq 194$ have been investigated. In [14,15,47], the analysis on the shape phase transition behaviors from the prolate to γ -unstable then to the oblate shape in several lower excited states of the even–even Pt isotopes was made by using the CQ Hamiltonian without configuration mixing. The IBM-2 model calculation for the even–even Pt isotopes was reported in [48], in which only the level energies up to 8_1^+ state in the yrast band and a few excited states in the quasi- β and quasi- γ band and the electric quadrupole moment of 2_1^+ state were fitted, where the yrast band consists of a series of the lowest energy levels for given quantum number of the angular momentum. In these Pt isotopes, configuration mixing with intruder excitation is likely to occur. A comparison and analysis of the model with and without configuration mixing are made in [49], in which possible intruder states in the excitation spectra of Pt isotopes are pointed out. In [17], the configuration mixing calculation of the low-lying spectrum of ^{194}Pt is carried out in the γ -soft rotor model, in which the O(6) quadrupole operators are used. The results show that the γ -soft rotor model fitting results to the low-lying level energies and the electric quadrupole moments are much improved.

As an example of the modified soft rotor model application, the low-lying excitation spectra and the electromagnetic transitional properties of even–even $^{176–198}\text{Pt}$ are fitted and compared to the experimental data and the results of the consistent-Q formalism, in which the configuration mixing is not considered for simplicity.

Since the IBM is equivalent to the valence shell model calculation, it is only suitable to describe low-lying positive parity states of medium and heavy even–even nuclei except for 1^+ states, which are due to the proton–neutron coupling or cross-shell particle–hole excitation. Hence, in this work, except 1^+ levels, only low-lying positive-parity level energies and related electromagnetic properties of even–even $^{176–198}\text{Pt}$ are considered. Moreover, experimentally measured level energies in smaller mass Pt are fewer, which also limits the number of levels to be fitted. In this work, the highest level energy E_{\max} to be fitted in even–even $^{176–198}\text{Pt}$ are set as follows: $E_{\max} = 0.91$ MeV for ^{176}Pt , $E_{\max} = 0.8$ MeV for ^{178}Pt , $E_{\max} = 1.2$ MeV for ^{180}Pt , $E_{\max} = 1.3$ MeV for ^{182}Pt , $E_{\max} = 1.06$ MeV for ^{184}Pt , $E_{\max} = 0.935$ MeV for ^{186}Pt , $E_{\max} = 1.7$ MeV for ^{188}Pt , $E_{\max} = 2.08$ MeV for ^{190}Pt , $E_{\max} = 1.95$ MeV for ^{192}Pt , $E_{\max} = 2.6$ MeV for ^{194}Pt , $E_{\max} = 2.3$ MeV for ^{196}Pt , and $E_{\max} = 2.1$ MeV for ^{198}Pt .

The modified soft rotor model has seven parameters. In order to reveal the influences of the modified soft rotor terms, the present model results are compared with those of the CQ formalism, which only has three parameters. The parameters of the present model and those of the CQ formalism adopted after best fits are shown in Tables 1 and 2, respectively, in which the corresponding boson number is also provided. As shown in Table 1, the parameter ξ in the exponential is a very small quantity, but very sensitive to the excitation energy of the states with higher angular momentum. The exponential term effectively brings the excitation energy of the states with higher angular momentum closer to the corresponding experimental value. Furthermore, although the model parameters of higher-order terms are small, the energy contribution of these higher-order terms to the excitation energies is still significant. Therefore, relatively larger values of the parameters of the CQ formalism with only one- and two-body interactions are required as shown in Table 2. It is also noticeable that the parameters c or c_0 and η of both the models are not continuous functions of the mass number, which is consistent to the description of $^{174–200}\text{Pt}$ shown in [14,15,47,50], in which $^{174–186}\text{Pt}$ and $^{188–200}\text{Pt}$ are grouped separately with the parameters in each group as continuous functions of the mass number A . Specifically, $^{176–186}\text{Pt}$ are near to the critical point of the spherical to prolate shape, for which η varies in the range $\eta \in [0.45, 0.48]$, while η becomes smaller in $^{188–198}\text{Pt}$ with $\eta \in [0.11, 0.19]$, indicating that the quadrupole deformation of these nuclei becomes larger. In addition, the three- and four-body interactions become more important in $^{188–198}\text{Pt}$ in the present model indicating the emergence of soft triaxiality in these nuclei.

Table 1. The parameters of the modified soft rotor model determined by the best fit to the excitation energies of $^{176–198}\text{Pt}$.

Nucleus	ξ	c_0 (MeV)	η	a_1	a_2	a_3	χ	N
$^{78}\text{Pt}_{98}$	−0.008	0.6216	0.4795	0	0	0.1287	−1.1218	10
$^{78}\text{Pt}_{100}$	0	0.8363	0.4594	0	0	0.1841	−1.0001	11
$^{78}\text{Pt}_{102}$	0.0002	0.9624	0.4483	−0.0449	0	0.0499	−0.8625	12
$^{78}\text{Pt}_{104}$	0.0006	0.9996	0.4462	0	−0.1648	0	−0.6456	13
$^{78}\text{Pt}_{106}$	0.0007	0.9481	0.4530	0.1747	−0.0775	0.2886	−0.6085	12
$^{78}\text{Pt}_{108}$	0.001	0.8079	0.4690	0	−0.2471	0	−0.4868	11
$^{78}\text{Pt}_{110}$	0.0011	1.0696	0.1061	−0.2197	−0.5142	0	−0.0159	10
$^{78}\text{Pt}_{112}$	0.00201	1.0708	0.1225	−0.3707	−0.2638	0.1009	0.0265	9
$^{78}\text{Pt}_{114}$	0.0009	1.0514	0.1389	−0.2587	−0.4614	0.2395	0.0635	8
$^{78}\text{Pt}_{116}$	0.0014	1.0113	0.1553	−0.2083	−0.3281	0.2547	0.0741	7
$^{78}\text{Pt}_{118}$	0.001	0.9507	0.1717	−0.2007	−0.3380	0.2777	0.0846	6
$^{78}\text{Pt}_{120}$	0.00148	0.8694	0.1882	−0.2085	−0.3810	0.2553	0.0953	5

Table 2. The parameters of the CQ Hamiltonian determined by the best fit to the excitation energies of $^{176-198}\text{Pt}$.

Nucleus	<i>c</i> (MeV)	η	χ	<i>N</i>
$^{176}\text{Pt}_{98}$	0.9814	0.5240	−1.2382	10
$^{178}\text{Pt}_{100}$	1.0296	0.4761	−1.1959	11
$^{180}\text{Pt}_{102}$	1.0402	0.4457	−0.9631	12
$^{182}\text{Pt}_{104}$	1.0133	0.4329	−0.7461	13
$^{184}\text{Pt}_{106}$	0.9490	0.4376	−0.7302	12
$^{186}\text{Pt}_{108}$	0.8471	0.4598	−0.6456	11
$^{188}\text{Pt}_{110}$	1.3784	0.3609	−0.1058	10
$^{190}\text{Pt}_{112}$	1.7264	0.2848	−0.0212	9
$^{192}\text{Pt}_{114}$	1.9379	0.2182	0.0159	8
$^{194}\text{Pt}_{116}$	2.0130	0.1612	0.0688	7
$^{196}\text{Pt}_{118}$	1.9515	0.1138	0.1111	6
$^{198}\text{Pt}_{120}$	1.7535	0.0759	0.1217	5

In order to reduce the adjustable parameters of the model, a polynomial of the mass number A fit to the parameters c_0 and η is made, from which these two parameters can be expressed in terms of the mass number A as

$$c_0 = \begin{cases} -365.851 + 4.03488A - 0.0110946A^2, & 176 \leq A \leq 186, \\ -91.0528 + 0.97428A - 0.00257589A^2, & 188 \leq A \leq 198, \end{cases}$$

$$\eta = \begin{cases} 37.5408 - 0.408827A + 0.00112643A^2, & 176 \leq A \leq 186, \\ -1.43657 + 0.00820571A, & 188 \leq A \leq 198, \end{cases}$$

which are quite similar to the empirical formulae shown in [15]. Similarly, the parameters c and η in the CQ formalism are expressed as

$$c = \begin{cases} -150.104 + 1.68344A - 0.0046875A^2, & 176 \leq A \leq 186, \\ -640.823 + 6.62379A - 0.0170629A^2, & 188 \leq A \leq 198, \end{cases}$$

$$\eta = \begin{cases} 73.3809 - 0.799588A + 0.00219107A^2, & 176 \leq A \leq 186, \\ 50.2558 - 0.490327A + 0.00119643A^2, & 188 \leq A \leq 198. \end{cases}$$

The fitting quality of the two models is measured by

$$\sigma(E) = \left(\frac{1}{N_0 - N_{\text{par}}} \sum_{i=1}^{N_0} (E_{i,\text{theor}} - E_{i,\text{expt}})^2 \right)^{1/2} \quad (17)$$

where N_{par} is the number of parameters, N_0 is the total number of level energies to be fitted, $E_{i,\text{theor}}$ and $E_{i,\text{expt}}$ are the level energies of the theory and the corresponding experimental data, respectively. The root-mean-square deviation of the fitting result to the excitation energies of $^{176-198}\text{Pt}$ under E_{max} is $\sigma(E) = 0.215$ MeV in the present model, while $\sigma(E) = 0.768$ MeV in the CQ formalism, indicating that the fitting quality of the present model is much better, which manifests the high-order interactions included in the modified soft rotor model are of importance.

The low-lying levels of $^{176-198}\text{Pt}$ are presented in Figure 2, in which the corresponding levels obtained from the present model and the CQ formalism (CQ) are also shown. It is shown that the fitting quality becomes better and the number of levels to be fitted becomes more with the increasing of the mass number. In comparison to the CQ formalism, the fitting quality of the present model in the ground-state band of $^{176-186}\text{Pt}$ is better. As the mass number increases, the fitting quality of the present model is significantly better than the CQ formalism for $^{188-198}\text{Pt}$, which implies that higher-order interactions play important roles in these nuclei. The fitting results show that $^{176-186}\text{Pt}$ are in the vibration-prolate phase

transitional region, and $^{188-190}\text{Pt}$ are in the U(5)-O(6) transitional region, while $^{192,194,196}\text{Pt}$ is near to the O(6) limit (γ -unstable) point, which is consistent with the previous conclusions shown in [49,51].

Experimentally, the 0_2^+ level is lower than that of 4_1^+ in ^{198}Pt , which is a characteristic in the U(5) (vibrational) spectrum. Thus, ^{198}Pt seems closer to the three-phase coexistence point with both spherical vibration and unstable triaxial deformation. The obvious shortcoming of the present model is that the 0_2^+ level of $^{192-196}\text{Pt}$ is lower than the corresponding experimental value. In addition, the 0_2^+ state of $^{176-188}\text{Pt}$ may be an intruder state as analyzed in [52–54]. Except the 0_2^+ level of ^{176}Pt , which is higher than the experimental value, the other level energies of $^{178-188}\text{Pt}$ with the excitation energy less than E_{\max} are well-fitted. Moreover, the 0_4^+ state of ^{192}Pt may be an intruder state [51]. Similarly, the 0_4^+ , 2_7^+ and 2_{11}^+ states of ^{194}Pt may also be the intruder states [17]. These possible intruder level energies are higher than E_{\max} and not considered in the present work.

Figure 3 shows the evolution behaviors of the 2_1^+ , 4_1^+ , 0_2^+ , 2_2^+ , 6_1^+ levels of $^{176-198}\text{Pt}$ in the present model and the CQ formalism. As shown in Figure 3, though the deviation of the CQ formalism is larger, the evolution behaviors of these levels revealed from both the models follow the experimental data pattern except for the 0_2^+ level.

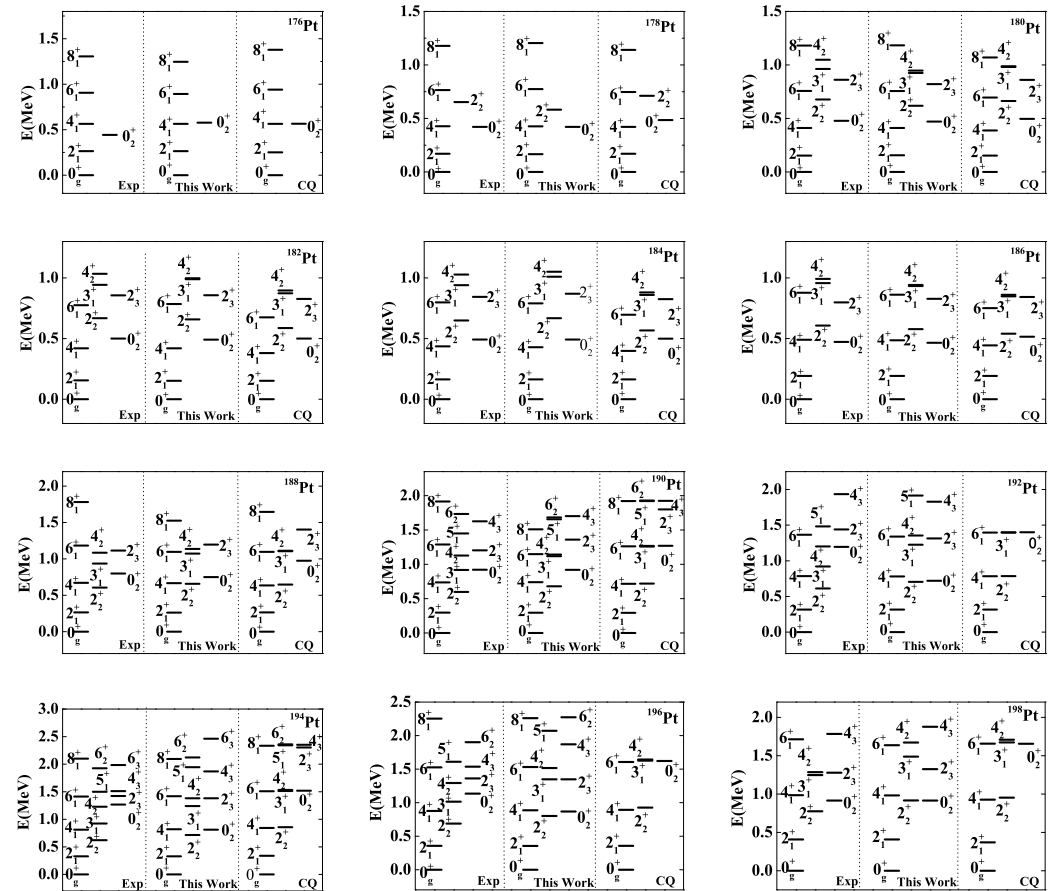


Figure 2. The low-lying energies of even-even $^{176-198}\text{Pt}$. The experimental data are taken from [55–66].

As shown in [8,9], several energy ratios are useful order parameters in elucidating the shape phase transitions, which are

$$R_{4/2} = \frac{E(4_1^+)}{E(2_1^+)}, \quad R_{2/1} = \frac{E(2_2^+)}{E(2_1^+)}, \quad R_{0/2} = \frac{E(0_2^+)}{E(2_1^+)}. \quad (18)$$

For example, in both the IBM and the collective model [8,9], $R_{4/2} = 10/3$ when the nuclear shape is prolate or oblate, $R_{4/2} = 2.5$ when the shape is γ -unstable, and $R_{4/2} = 2$ when the shape is near spherical. The energy ratios $R_{4/2}$, $R_{2/1}$, and $R_{0/2}$ of $^{176-198}\text{Pt}$ are presented in Figure 4, which clearly shows that $R_{4/2}$ and $R_{2/1}$ obtained from the present model are closer to the experimental data. It can be observed that, with the increasing of the mass number A, these Pt nuclei evolve from the spherical shape with $R_{4/2} \sim 2.15$ to the γ -soft triaxial shape with $R_{4/2} \sim 2.4$. Though the $R_{0/2}$ curves of both the models roughly follow the experimental data pattern, there are significant deviations from the corresponding experimental data, especially those of $^{188-198}\text{Pt}$, which should be further improved.

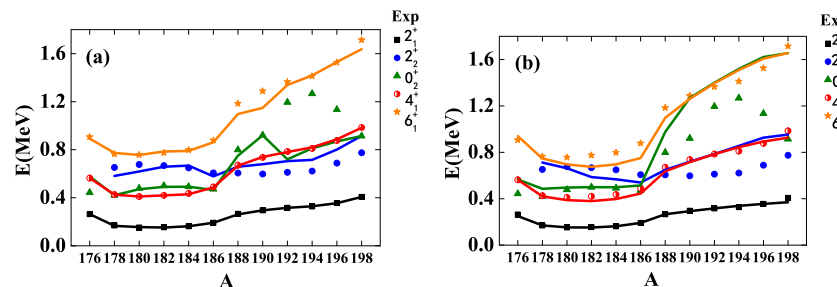


Figure 3. The low-lying level energies of even-even $^{176-198}\text{Pt}$ as functions of the mass number A. (a) The present model; (b) the CQ formalism.

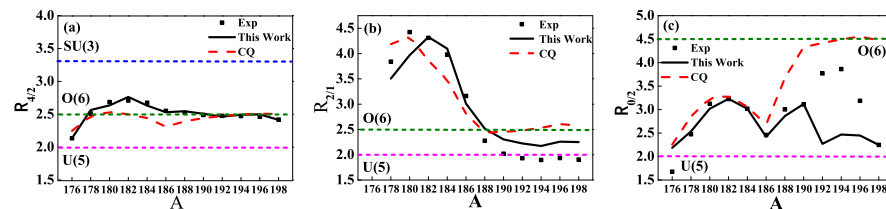


Figure 4. The energy ratios of even-even $^{176-198}\text{Pt}$ as functions of the mass number A. (a) $R_{4/2}$; (b) $R_{2/1}$; (c) $R_{0/2}$, where the horizontal dotted lines from the top to the bottom are the values at the SU(3), the O(6), and the U(5) limit, respectively, accept for panel (c), in which the SU(3) limit value is too large and not included.

Besides the level energies, E2 transition rates and electric quadrupole moments are also the key quantities to be analyzed. Once the model parameters are determined in fitting to the level energies, the effective boson charge parameter q_2 is determined by the experimental $B(E2; 2_1^+ \rightarrow 0_1^+)$ except for ^{178}Pt , which is determined by the experimental $B(E2; 4_1^+ \rightarrow 2_1^+)$ because the experimental $B(E2; 2_1^+ \rightarrow 0_1^+)$ of ^{178}Pt is unavailable. The theoretical and the corresponding experimental $B(E2)$ values of $^{176-198}\text{Pt}$ for several transitions among the excited states concerned are shown in Tables 3 and 4, in which the standard deviations of the experimental results are given in parentheses on the right side of the corresponding experimental values. The underlined theoretical value indicating the effective boson charge parameter q_2 is determined by the corresponding experimental value. Except for a few inter-band transitions, the E2 transition rates within the yrast band are well fit by both the models.

Table 3. Some $B(E2)$ values (in W.u.) and the corresponding half-lives (in ps) of $^{176-186}\text{Pt}$ calculated from the present model and the CQ formalism. The experimental data are taken from [55–63], where the symbol “–” indicates that the corresponding value is experimentally not available.

	$L_\zeta \longrightarrow L'_{\zeta'}$	$B_{\text{Exp}}(E2)$	$B_{\text{This Work}}(E2)$	$B_{\text{CQ}}(E2)$	$(T_{1/2})_{\text{Exp}}$	$(T_{1/2})_{\text{This Work}}$	$(T_{1/2})_{\text{CQ}}$
^{176}Pt	$2^+_1 \rightarrow 0^+_1$	87(8)	<u>87.011</u>	<u>87.008</u>	76	130.180	130.184
	$4^+_1 \rightarrow 2^+_1$	163(15)	148.646	159.366	22.2	40.214	37.509
	$6^+_1 \rightarrow 4^+_1$	174(16)	191.204	197.981	11.2	16.237	15.681
	$8^+_1 \rightarrow 6^+_1$	192(25)	217.843	215.919	4.7	6.512	6.570
^{178}Pt	$4^+_1 \rightarrow 2^+_1$	195(17)	<u>195.068</u>	<u>195.009</u>	37.5	65.430	65.450
	$6^+_1 \rightarrow 4^+_1$	186(14)	231.816	232.173	10.9	13.993	13.971
	$8^+_1 \rightarrow 6^+_1$	206(23)	248.684	249.205	–	4.789	4.779
^{180}Pt	$2^+_1 \rightarrow 0^+_1$	154(15)	<u>154.051</u>	<u>154.027</u>	374	1091.599	1091.769
	$4^+_1 \rightarrow 2^+_1$	3.1×10^2 (4)	247.620	251.145	22.9	49.808	49.109
	$6^+_1 \rightarrow 4^+_1$	≥50	290.043	296.687	≤35	9.662	9.446
^{182}Pt	$2^+_1 \rightarrow 0^+_1$	114(8)	<u>114.002</u>	<u>114.004</u>	479	1361.953	1361.929
	$4^+_1 \rightarrow 2^+_1$	192(12)	176.723	184.507	32.5	61.294	58.708
	$6^+_1 \rightarrow 4^+_1$	292(20)	203.217	219.257	5.28	12.124	11.237
^{184}Pt	$2^+_1 \rightarrow 0^+_1$	127(5)	<u>127.009</u>	<u>127.014</u>	360	936.807	936.770
	$2^+_3 \rightarrow 0^+_1$	>0.0100	2.960	1.385	≤0.0015	10.800	23.081
	$2^+_3 \rightarrow 0^+_2$	>0.095	47.809	74.740	≤0.0015	52.991	33.897
	$4^+_1 \rightarrow 2^+_1$	210(8)	202.506	207.042	25.3	44.583	43.606
	$6^+_1 \rightarrow 4^+_1$	226(12)	236.014	246.825	6.1	9.331	8.923
	$8^+_1 \rightarrow 6^+_1$	271(18)	251.128	267.136	2.15	3.623	3.406
	$2^+_1 \rightarrow 0^+_1$	94(5)	<u>94.010</u>	<u>94.426</u>	240	550.146	547.722
^{188}Pt	$2^+_1 \rightarrow 0^+_1$	89(4)	<u>89.167</u>	<u>89.014</u>	66	112.028	112.220
	$4^+_1 \rightarrow 2^+_1$	150(+4-5)	117.39	129.247	5.1	10.400	9.446
	$6^+_1 \rightarrow 4^+_1$	158(15)	132.752	148.733	1.53	2.820	2.517
	$8^+_1 \rightarrow 6^+_1$	118(17)	137.830	155.836	0.97	1.262	1.116
^{190}Pt	$2^+_1 \rightarrow 0^+_1$	56(3)	<u>56.010</u>	<u>56.018</u>	62.3	103.070	103.055
^{192}Pt	$2^+_1 \rightarrow 0^+_1$	57.2(12)	<u>57.199</u>	<u>57.198</u>	43.7	70.653	70.654
	$2^+_2 \rightarrow 0^+_1$	0.55(4)	1.911	0.004	26.5	78.849	37,670.042
	$2^+_2 \rightarrow 2^+_1$	109(7)	69.760	77.975	26.5	81.611	73.013
	$4^+_1 \rightarrow 2^+_1$	89(5)	77.345	78.108	4.2	7.450	7.377
	$3^+_1 \rightarrow 2^+_1$	0.68(7)	1.525	0.007	21.3	105.526	22,989.550
	$3^+_1 \rightarrow 2^+_2$	102(10)	46.093	60.795	21.3	101.257	76.770
	$6^+_1 \rightarrow 4^+_1$	70(30)	84.382	84.901	1.8	2.316	2.302
	$3^+_1 \rightarrow 4^+_1$	38(10)	26.257	24.342	21.3	10,589.454	11,422.533

Table 4. The same as Table 3, but for $^{194-198}\text{Pt}$. The experimental data are taken from [64–67].

	$L_\zeta \longrightarrow L'_{\zeta'}$	$B_{\text{Exp}}(E2)$	$B_{\text{This Work}}(E2)$	$B_{\text{CQ}}(E2)$	$(T_{1/2})_{\text{Exp}}$	$(T_{1/2})_{\text{This Work}}$	$(T_{1/2})_{\text{CQ}}$
^{194}Pt	$2^+_1 \rightarrow 0^+_1$	49.2(8)	<u>49.214</u>	<u>49.205</u>	41.7	68.261	68.274
	$2^+_2 \rightarrow 0^+_1$	0.29(4)	1.008	0.137	35	135.900	999.908
	$2^+_2 \rightarrow 2^+_1$	89(11)	62.116	63.507	35	93.474	91.427
	$4^+_1 \rightarrow 2^+_1$	85(5)	65.238	66.106	3.7	7.437	7.339
	$4^+_1 \rightarrow 2^+_1$	0.36(7)	1.279	0.0003	3.8	16.793	71,595.730
	$4^+_2 \rightarrow 2^+_2$	21(4)	36.687	36.299	3.8	4.219	4.229
	$4^+_2 \rightarrow 4^+_1$	14	24.721	31.944	3.8	40.428	31.287
	$0^+_2 \rightarrow 2^+_1$	0.63(14)	3.269	0.396	6.1	5.344	44.117
	$0^+_2 \rightarrow 2^+_2$	8.4(19)	87.311	67.085	6.1	1.308	1.703
	$3^+_1 \rightarrow 4^+_1$	<75	21.289	19.870	–	35,551.848	38,090.754
	$3^+_1 \rightarrow 2^+_2$	100	42.538	50.148	–	121.345	102.931
	$3^+_1 \rightarrow 2^+_1$	<0.64	0.766	0.190	–	225.150	907.709

Table 4. *Cont.*

	$L_\xi \rightarrow L'_\xi'$	$B_{\text{Exp}}(E2)$	$B_{\text{This Work}}(E2)$	$B_{\text{CQ}}(E2)$	$(T_{1/2})_{\text{Exp}}$	$(T_{1/2})_{\text{This Work}}$	$(T_{1/2})_{\text{CQ}}$
^{194}Pt	$6_1^+ \rightarrow 4_1^+$	67(21)	69.313	69.965	1.6	2.347	2.325
	$8_1^+ \rightarrow 6_1^+$	50(14)	64.454	66.068	1.1	1.284	1.252
	$8_2^+ \rightarrow 6_2^+$	53(10)	40.362	42.628	0.61	1.222	1.157
^{196}Pt	$2_1^+ \rightarrow 0_1^+$	40.60(20)	40.608	40.605	34.15	54.244	54.248
	$2_2^+ \rightarrow 0_1^+$	$4 \times 10^{-6}(4)$	1.373	0.309	33.8	59.081	262.519
	$2_2^+ \rightarrow 0_2^+$	5(5)	0.003	11.079	—	7,121,171.886	1928.289
	$2_3^+ \rightarrow 0_1^+$	0.0025(24)	0.064	0.033	—	42.145	81.735
	$0_2^+ \rightarrow 2_2^+$	18(10)	69.587	51.888	4.2	10.143	13.602
	$0_2^+ \rightarrow 2_1^+$	2.8(15)	3.072	0.545	4.2	14.201	80.047
	$0_3^+ \rightarrow 2_1^+$	<5.0	1.046	0.380	1.6	9.571	26.345
	$0_3^+ \rightarrow 2_2^+$	<0.41	0.009	1.218	1.6	7541.910	55.728
	$2_2^+ \rightarrow 2_1^+$	54(+11-12)	45.337	50.195	33.8	31.224	28.203
	$2_3^+ \rightarrow 2_2^+$	0.26(23)	0.277	0.086	—	329.352	1060.819
	$4_1^+ \rightarrow 2_1^+$	60.0(9)	53.551	53.566	3.55	6.127	6.125
	$4_2^+ \rightarrow 2_2^+$	29(+6-29)	28.837	28.323	2.6	5.389	5.487
	$4_2^+ \rightarrow 2_1^+$	0.56(+12-17)	0.691	0.002	2.6	25.103	8673.028
	$2_3^+ \rightarrow 4_1^+$	0.13(12)	0.600	0.370	—	782.267	1268.541
	$4_2^+ \rightarrow 4_1^+$	17(6)	18.093	23.829	2.6	55.878	42.427
	$6_1^+ \rightarrow 4_1^+$	73(+4-73)	54.709	54.661	0.98	2.000	2.001
	$6_3^+ \rightarrow 4_1^+$	0.48(14)	0.029	0.0003	0.77	234.695	22,687.186
	$6_3^+ \rightarrow 4_2^+$	49(13)	0.036	0.008	0.77	1885.478	8484.649
	$6_3^+ \rightarrow 6_1^+$	16(5)	0.007	0.020	0.77	69,886.211	24,460.174
	$8_1^+ \rightarrow 6_1^+$	78(+10-78)	47.562	48.542	0.42	1.304	1.278
^{198}Pt	$2_1^+ \rightarrow 0_1^+$	31.81(22)	31.813	31.818	22.25	34.950	34.945
	$2_2^+ \rightarrow 0_1^+$	0.038(12)	1.035	0.148	27	42.912	300.093
	$2_3^+ \rightarrow 0_1^+$	0.05(3)	0.066	0.009	9.7	54.756	401.545
	$2_3^+ \rightarrow 2_1^+$	0.6(4)	0.003	0.0001	9.7	8209.613	246,288.402
	$2_3^+ \rightarrow 2_2^+$	2.2(15)	0.469	0.060	9.7	806.114	6301.127
	$2_2^+ \rightarrow 2_1^+$	37(7)	34.484	37.277	27	54.085	50.033
	$0_2^+ \rightarrow 2_1^+$	26(7)	2.225	0.302	—	166.593	1227.382
	$4_1^+ \rightarrow 2_1^+$	38(4)	40.519	40.567	3.3	4.750	4.745
	$6_1^+ \rightarrow 4_1^+$	>57	38.899	39.092	≤ 0.7	1.550	1.543

In addition, the half-lives (in second) due to E2 decay in the IBM can be estimated by [68]

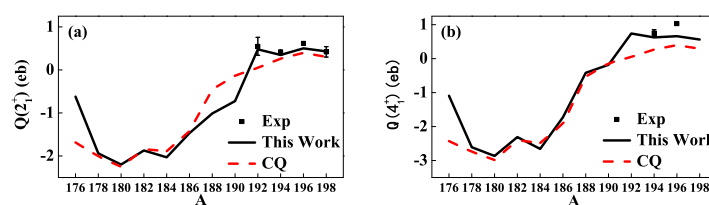
$$(T_{1/2})_{\text{IBM}} = \frac{1}{1.23 \times 10^9 \times E_\gamma^5 \times \ln 2 \times B_{\text{IBM}}(E2)} \quad (19)$$

based on the standard definition [69], where E_γ (in MeV) is the transition energy between the two levels, and the unit of $B(E2)$ is $e^2 \text{fm}^4$. As shown in Tables 3 and 4, though there are obvious deviations in the $T_{1/2}$ values, except for a few exceptions, the data pattern of the results of this work and those of the the CQ formalism roughly follow that of the experimental data.

The quadrupole moments of some low-lying states of $^{192-198}\text{Pt}$ obtained from both the models and the corresponding experimental data are shown in Table 5. It can be observed that $Q(2_1^+)$ and $Q(4_1^+)$ values of the present model are closer to the corresponding experimental results, but deviations in the values of other states from the experimental data are noticeable. Though the experimental data of $^{176-198}\text{Pt}$ are still absent, the evolution behaviors of $Q(2_1^+)$ and $Q(4_1^+)$ as functions of the mass number A are shown in Figure 5, which indicates the shape evolution from prolate to oblate with the increasing of the mass number.

Table 5. Some quadrupole moments (in eb) of $^{188-194}\text{Pt}$. The experimental data are taken from [63–66].

		Experiment	This Work	CQ
^{192}Pt	$Q(2_1^+)$	+0.55(21)	+0.478	+0.051
^{194}Pt	$Q(2_1^+)$	+0.409($^{+62}_{-43}$)	+0.348	+0.267
	$Q(2_2^+)$	-0.303($^{+93}_{-37}$)	-0.322	-0.249
	$Q(4_1^+)$	+0.752($^{+92}_{-105}$)	+0.624	+0.268
	$Q(4_2^+)$	-0.06(11)	+0.111	-0.106
	$Q(6_1^+)$	+0.195($^{+85}_{-188}$)	+0.794	+0.263
	$Q(8_1^+)$	-0.06, 0.28	+0.908	+0.262
^{196}Pt	$Q(2_1^+)$	+0.62	+0.503	+0.399
	$Q(2_2^+)$	-0.39	-0.474	-0.372
	$Q(4_1^+)$	+1.03	+0.662	+0.397
	$Q(6_1^+)$	-0.18	+0.762	+0.380
^{198}Pt	$Q(2_1^+)$	+0.42(12), 0.54(12)	+0.431	+0.305

**Figure 5.** The electric quadrupole moments of even–even $^{176-198}\text{Pt}$ as functions of the mass number A. (a) $Q(2_1^+)$; (b) $Q(4_1^+)$.

In order to reveal the shape evolution of $^{176-198}\text{Pt}$ further, the polar coordinates are used to plot the parameter evolution within the extended Casten triangle shown in Figure 1, which is illustrated in Figure 6. The model parameters η and χ are converted into the radial and angular variables (ρ, θ) with

$$\rho = \frac{\sqrt{3}(1 - \eta)}{2 \cos \frac{\pi \chi}{3\sqrt{7}}}, \quad \theta = \frac{\pi}{6} + \frac{\pi \chi}{3\sqrt{7}}, \quad (20)$$

where $0 \leq \eta \leq 1$, $-\frac{\sqrt{7}}{2} \leq \chi \leq \frac{\sqrt{7}}{2}$, so that $0 \leq \rho \leq 1$ and $0^\circ \leq \theta \leq 60^\circ$. Thus, $\rho = 0$ and $\theta = 0$ correspond to the U(5) limit; $\rho = 1$ and $\theta = 0$ correspond to the SU(3) limit; $\rho = 1$ and $\theta = 60^\circ$ correspond to the $\overline{\text{SU}(3)}$ limit, $\rho = 0.866$ and $\theta = 30^\circ$ correspond to the O(6) limit. Furthermore, when $\theta = 0^\circ$ or 60° the parameter ρ changes within the closed interval $[0, 1]$, there exists the first-order phase transition from the U(5) limit to the SU(3) or $\overline{\text{SU}(3)}$ limit, of which the critical point is labeled as X(5) or $\overline{\text{X}(5)}$ in Figures 1 and 6. The corresponding value η_c is given by [26]

$$\eta_c = \frac{14}{28 + \chi_c^2} = 0.4707 \quad (21)$$

with $\chi_c = \mp \frac{\sqrt{7}}{2}$. Similarly, there is the critical point of U(5)-O(6) transition with $\rho = \sqrt{3}/4$ and $\theta = 30^\circ$, of which the point in the extended Casten triangle is labeled as E(5). By using (20), the trajectories of these even–even Pt isotopes determined by the two parameters of both the models in the extended Casten triangle are shown in Figure 7. It can be seen that the two discontinuous trajectories determined by the two models are quite similar to the previous results [14]. The reason that the evolution trajectory of $^{188-198}\text{Pt}$ in the present model is in opposite direction of that in the CQ formalism is due to the significant contribution of the third and fourth order terms involved in the present model, as clearly shown by the parameters presented in Table 1.

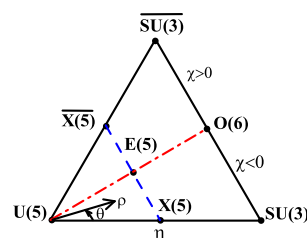


Figure 6. The extended Casten triangle in the polar coordinates.

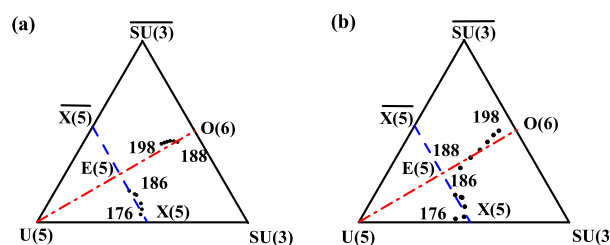


Figure 7. $^{176-198}\text{Pt}$ evolution trajectories in the extended Casten triangle. (a) The present model; (b) the CQ formalism.

5. Conclusions

Based on the IBM CQ formalism, the exponential type modification to the strength of the quadrupole–quadrupole interaction with three- and four-body interactions are introduced. As an example of the model application, low-lying positive-parity level energies, the related $B(E2)$ values, and some electric quadrupole moments of even–even $^{176-198}\text{Pt}$ are fitted and compared to the experimental data and the results of the consistent-Q formalism.

The results show that the exponential modification to the quadrupole–quadrupole interaction effectively reduces the excitation energies of excited states with higher angular momentum in accordance to the experimental data, which cannot be achieved in the original consistent-Q formalism. The higher-order interactions introduced in the present model make the level energies of the ground-state band and the quasi- γ band much improved, especially in the isotopes with large mass number, so that the fitting results of level energies of these nuclei are significantly improved, indicating that the high-order interactions are of importance in these nuclei. Though the $B(E2)$ values of the transitions within the yrast band are all well fit by both the models, the electric quadrupole moments $Q(2_1^+)$ and $Q(4_1^+)$ obtained from the present model are also significantly better than those obtained from the CQ formalism. However, deviations in quadrupole moments of other states from the experimental data are still noticeable. According to the fitting results, the shape evolution of even–even $^{176-198}\text{Pt}$ is revealed through the typical low-lying energy ratios $R_{4/2}$, $R_{2/1}$, $R_{0/2}$ and the electric quadrupole moments $Q(2_1^+)$, $Q(4_1^+)$. The trajectories in the extended Casten triangle are also determined. Though the discontinuous evolution trajectories determined by the present model are quite similar to those of the CQ formalism, namely, $^{176-186}\text{Pt}$ are near the X(5)-E(5) critical line, while $^{188-198}\text{Pt}$ are near the E(5)-O(6) critical line with triaxial γ -unstable shape, the evolution trajectory of $^{188-198}\text{Pt}$ in the present model is in the opposite direction of that in the CQ formalism, which is due to the significant contribution of the three- and four-body terms involved in the present model.

Although the present model improves the CQ formalism, besides deviations in some quadrupole moments, the 0_2^+ level in the quasi- β band is still lower than the experimental result of the nuclei with larger mass number, which may be due to the occurrence of cross-shell particle-hole excitation in these nuclei. To improve the model further, it is necessary to consider multi-particle and multi-hole excitations with configuration mixing, which may be studied in our future work.

Author Contributions: Methodology, F.P. and T.W.; numerical calculations and analyses, D.L. and T.W.; writing—original draft, D.L. and T.W.; writing—review and editing, F.P.; plus senior leadership and oversight, T.W. and F.P. All authors have read and agreed to the final version of the manuscript.

Funding: This research was funded by the National Natural Science Foundation of China (12175097); and Science and Technology Research Planning Project of Education Department of Jilin Province (JKH20210526KJ).

Institutional Review Board Statement: Not applicable.

Informed Consent Statement: Not applicable.

Data Availability Statement: The Fortran code for the model calculation and the results presented are available upon request.

Conflicts of Interest: The authors have no conflict of interest.

References

1. Arima, A.; Iachello, F. Collective nuclear states as representations of a SU(6) group. *Phys. Rev. Lett.* **1975**, *35*, 1069–1072. [\[CrossRef\]](#)
2. Arima, A.; Iachello, F. Interacting boson model of collective states I. The vibrational Limit. *Ann. Phys.* **1976**, *99*, 253–317. [\[CrossRef\]](#)
3. Arima, A.; Iachello, F. Interacting boson model of collective states II. The rotational limit. *Ann. Phys.* **1978**, *111*, 201–238. [\[CrossRef\]](#)
4. Arima, A.; Iachello, F. Interacting boson model of collective states III. The transition from SU(5) to SU(3). *Ann. Phys.* **1978**, *115*, 325–366. [\[CrossRef\]](#)
5. Arima, A.; Iachello, F. Interacting boson model of collective states IV. The O(6) limit. *Ann. Phys.* **1979**, *123*, 468–492. [\[CrossRef\]](#)
6. Iachello, F.; Arima, A. *The Interacting Boson Model*; Cambridge University: Cambridge, UK, 1987.
7. Casten, R.F.; Warner, D.D. The interacting boson approximation. *Rev. Mod. Phys.* **1988**, *60*, 389–469. [\[CrossRef\]](#)
8. Casten, R.F. Quantum phase transitions and structural evolution in nuclei. *Prog. Part. Nucl. Phys.* **2009**, *62*, 183–209. [\[CrossRef\]](#)
9. Cejnar, P.; Jolie, J.; Casten, R.F. Quantum phase transitions in the shapes of atomic nuclei. *Rev. Mod. Phys.* **2010**, *82*, 2155–2212. [\[CrossRef\]](#)
10. Fortunato, L. Quantum phase transitions in algebraic and collective models of nuclear structure. *Prog. Part. Nucl. Phys.* **2021**, *121*, 103891. [\[CrossRef\]](#)
11. Böyükata, M.; Alonso, C.E.; Arias, J.M.; Fortunato, L.; Vitturi, A. Review of shape phase transition studies for Bose-Fermi systems, The effect of the odd-particle on the bosonic core. *Symmetry* **2021**, *13*, 215. [\[CrossRef\]](#)
12. Parker, M.C.; Jeynes, C.; Catford, W.N. Halo properties in helium nuclei from the perspective of geometrical thermodynamics. *Ann. Phys.* **2022**, *534*, 2100278. [\[CrossRef\]](#)
13. Chen, J.Q. Nucleon-pair shell model, Formalism and special cases. *Nucl. Phys. A* **1997**, *626*, 686–714. [\[CrossRef\]](#)
14. McCutchan, E.A.; Casten, R.F.; Zamfir, N.V. Simple interpretation of shape evolution in Pt isotopes without intruder states. *Phys. Rev. C* **2005**, *71*, 061301(R). [\[CrossRef\]](#)
15. Pan, F.; Wang, T.; Huo, Y.-S.; Draayer, J.P. Quantum phase transitions in the consistent-Q Hamiltonian of the interacting boson model. *J. Phys. G, Nucl. Part. Phys.* **2008**, *35*, 125105. [\[CrossRef\]](#)
16. Tobin, G.K.; Ferriss, M.C.; Launey, K.D.; Draayer, J.P.; Drefuss, A.C.; Bahri, C. Symplectic no-core shell-model approach to intermediate-mass nuclei. *Phys. Rev. C* **2014**, *89*, 034312. [\[CrossRef\]](#)
17. Pan, F.; Yuan, S.L.; Qiao, Z.; Bai, J.C.; Zhang, Y.; Draayer, J.P. γ -soft rotor with configuration mixing in the O(6) limit of the interacting boson model. *Phys. Rev. C* **2018**, *97*, 034326. [\[CrossRef\]](#)
18. Smirnov, Y.F.; Smirnova, N.A.; Van Isacker, P. SU(3) realization of the rigid asymmetric rotor within the interacting boson model. *Phys. Rev. C* **2000**, *61*, 041302. [\[CrossRef\]](#)
19. Zhang, Y.; Pan, F.; Dai, L.R.; Draayer, J.P. Triaxial rotor in the SU(3) limit of the interacting boson model. *Phys. Rev. C* **2014**, *90*, 044310. [\[CrossRef\]](#)
20. Warner, D.D.; Casten, R.F.D. Revised formulation of the phenomenological interacting boson approximation. *Phys. Rev. Lett.* **1982**, *48*, 1385–1389. [\[CrossRef\]](#)
21. Warner, D.D.; Casten, R.F. Predictions of the interacting boson approximation in a consistent Q framework. *Phys. Rev. C* **1983**, *28*, 1798–1806. [\[CrossRef\]](#)
22. Jolie, J.; Cejnar, P.; Casten, R.F.; Heinze, S.; Linnemann, A.; Werner, V. Triple point of nuclear deformations. *Phys. Rev. Lett.* **2002**, *89*, 182502. [\[CrossRef\]](#) [\[PubMed\]](#)
23. Bohr, A.; Mottelson, B.R. *Nuclear Structure II*; World Scientific Publishing Company: Singapore, 1998.
24. Ginocchio, J.N.; Kirson, M.W. Relationship between the Bohr Collective Hamiltonian and the Interacting-Boson Model. *Phys. Rev. Lett.* **1980**, *44*, 1744–1747. [\[CrossRef\]](#)
25. Dieperink, A.E.L.; Scholten, O.; Iachello, F. Classical limit of the Interacting-Boson Model. *Phys. Rev. Lett.* **1980**, *44*, 1747–1750. [\[CrossRef\]](#)

26. Zhang, Y.; Zuo, Y.; Pan, F.; Draayer, J.P. Excited-state quantum phase transitions in the interacting boson model, Spectral characteristics of 0^+ states and effective order parameter. *Phys. Rev. C* **2016**, *93*, 044302. [\[CrossRef\]](#)

27. Iachello, F. Dynamic symmetries at the critical point. *Phys. Rev. Lett.* **2000**, *85*, 3580–3584. [\[CrossRef\]](#) [\[PubMed\]](#)

28. Iachello, F. Analytic description of critical point nuclei in a spherical-axially deformed shape phase transition. *Phys. Rev. Lett.* **2001**, *87*, 052502. [\[CrossRef\]](#)

29. Van Isacker, P.; Chen, J.Q. Classical limit of the interacting boson Hamiltonian. *Phys. Rev. C* **1981**, *24*, 684–689. [\[CrossRef\]](#)

30. Heyde, K.; Van Isacker, P.; Waroquier, M.; Moreau, J. Triaxial shapes in the interacting boson model. *Phys. Rev. C* **1984**, *29*, 1420–1427. [\[CrossRef\]](#)

31. Garcia-Ramos, J.E.; Alonso, C.E.; Arias, J.M.; Van Isacker, P. Anharmonic double- γ vibrations in nuclei and their description in the interacting boson model. *Phys. Rev. C* **2000**, *61*, 047305. [\[CrossRef\]](#)

32. Loewenich, K.; Zell, K.O.; Dewald, A.; Gast, W.; Gelberg, A.; Lieberz, W.; Von Brentano, P.; Van Isacker, P. In-beam spectroscopy of ^{120}Xe . *Nucl. Phys. A* **1986**, *468*, 361–372. [\[CrossRef\]](#)

33. Sorgunlu, B.; Van Isacker, P. Triaxiality in the interacting boson model. *Nucl. Phys. A* **2008**, *808*, 27–46. [\[CrossRef\]](#)

34. Vanthournout, J.; De Meyer, H.; Vanden Berghe, G. Symmetry-preserving higher-order terms in the O(6) limit of the interacting boson model. *Phys. Rev. C* **1988**, *38*, 414–418. [\[CrossRef\]](#) [\[PubMed\]](#)

35. Vanthournout, J. Influence of symmetry-conserving higher order interactions in the interacting boson model on the first β and γ band in rotational nuclei. *Phys. Rev. C* **1990**, *41*, 2380–2385. [\[CrossRef\]](#) [\[PubMed\]](#)

36. Van Isacker, P. Dynamical symmetry and higher-order interactions. *Phys. Rev. Lett.* **1999**, *83*, 4269–4272. [\[CrossRef\]](#)

37. Rowe, D.J.; Thiamova, G. The many relationships between the IBM and the Bohr model. *Nucl. Phys. A* **2005**, *760*, 59–81. [\[CrossRef\]](#)

38. Thiamova, G.; Cejnar, P. Prolate-oblate shape-phase transition in the O(6) description of nuclear rotation. *Nucl. Phys. A* **2006**, *765*, 97–111. [\[CrossRef\]](#)

39. Leschber, Y.; Draayer, J.P. Algebraic realization of rotational dynamics. *Phys. Lett. B* **1987**, *190*, 1–6. [\[CrossRef\]](#)

40. Castaños, O.; Draayer, J.P.; Leschber, Y. Shape variables and the shell model. *Z. Phys. A* **1988**, *329*, 33–43. [\[CrossRef\]](#)

41. Fortunato, L.; Alonso, C.E.; Arias, J.M.; García-Ramos, J.E.; Vitturi, A. Phase diagram for a cubic-Q interacting boson model Hamiltonian: Signs of triaxiality. *Phys. Rev. C* **2011**, *84*, 014326. [\[CrossRef\]](#)

42. Wang, T. New γ -soft rotation in the interacting boson model with SU(3) higher-order interactions. *Chin. Phys. C* **2022**, *46*, 074101. [\[CrossRef\]](#)

43. Wang, T. A collective description of the unusually low ratio $B_{4/2} = B(E2; 4_1^+ \rightarrow 2_1^+)/B(E2; 2_1^+ \rightarrow 1_1^+)$. *EPL* **2020**, *129*, 52001. [\[CrossRef\]](#)

44. Zhang, Y.; He, Y.W.; Karlsson, D.; Qi, C.; Pan, F.; Draayer, J.P. A theoretical interpretation of the anomalous reduced E2 transition probabilities along the yrast line of neutron-deficient nuclei. *Phys. Lett. B* **2022**, *834*, 137443. [\[CrossRef\]](#)

45. Rosensteel, G. Analytic formulae for interacting boson model matrix elements in the SU(3) basis. *Phys. Rev. C* **1990**, *41*, 730–735. [\[CrossRef\]](#)

46. Akiyama, Y.; Draayer, J.P. A user’s guide to fortran programs for Wigner and Racah coefficients of SU(3). *Comput. Phys. Commun.* **1973**, *5*, 405–406. [\[CrossRef\]](#)

47. McCutchan, E.A.; Zamfir, N.V. Simple description of light W, Os, and Pt nuclei in the interacting boson model. *Phys. Rev. C* **2005**, *71*, 054306. [\[CrossRef\]](#)

48. Bijker, R.; Dieperink, A.E.L.; Scholten, O.; Spanhoff, R. Description of the Pt and Os isotopes in the interacting boson model. *Nucl. Phys. A* **1980**, *344*, 207–232. [\[CrossRef\]](#)

49. García-Ramos, J.E.; Heyde, K. The Pt isotopes, Comparing the Interacting Boson Model with configuration mixing and the extended consistent-Q formalism. *Nucl. Phys. A* **2009**, *825*, 39–70. [\[CrossRef\]](#)

50. Thiamova, G. The IBM description of triaxial nuclei. *Eur. Phys. J. A* **2010**, *45*, 81–90. [\[CrossRef\]](#)

51. Gladnishki, K.A.; Petkov, P.; Dewald, A.; Fransen, C.; Hackstein, M.; Jolie, J.; Pissulla, T.; Rother, W.; Zell, K.O. Yrast electromagnetic transition strengths and shape coexistence in ^{186}Pt . *Nucl. Phys. A* **2012**, *877*, 19–34. [\[CrossRef\]](#)

52. Delion, D.S.; Florescu, A.; Huyse, M.; Wauters, J.; Van Duppen, P.; Insolia, A.; Liotta, R.J. Microscopic description of alpha decay to intruder 0_2^+ states in Pb, Po, Hg, and Pt isotopes. *Phys. Rev. Lett.* **1995**, *74*, 3939–3942. [\[CrossRef\]](#)

53. Garg, U.; Chaudhury, A.; Drigert, M.W.; Funk, E.G.; Mihelich, J.W.; Radford, D.C.; Helppi, H.; Holzmann, R.; Janssens, R.V.F.; Khoo, T.L.; et al. Life time measurements in ^{184}Pt and the shape coexistence picture. *Phys. Lett. B* **1986**, *180*, 319–323. [\[CrossRef\]](#)

54. Hebbinghaus, G.; Kutsarova, T.; Gast, W.; Krämer-Flecken, A.; Lieder, R.M.; Urban, W. Study of band structures in the γ -unstable nucleus ^{186}Pt . *Nucl. Phys. A* **1990**, *514*, 225–251. [\[CrossRef\]](#)

55. Basunia, M.S. Nuclear Data Sheets for $A = 176$. *Nucl. Data Sheets* **2006**, *107*, 791–1026. [\[CrossRef\]](#)

56. Achterberg, E.; Capurro, O.A.; Marti, G.V. Nuclear Data Sheets for $A = 178$. *Nucl. Data Sheets* **2009**, *110*, 1473–1688. [\[CrossRef\]](#)

57. McCutchan, E.A. Nuclear Data Sheets for $A = 180$. *Nucl. Data Sheets* **2015**, *126*, 151–372. [\[CrossRef\]](#)

58. Singh, B.; Roediger, J.C. Nuclear Data Sheets for $A = 182$. *Nucl. Data Sheets* **2010**, *111*, 2081–2330. [\[CrossRef\]](#)

59. Baglin, C.M. Nuclear Data Sheets for $A = 184$. *Nucl. Data Sheets* **2010**, *111*, 275–523. [\[CrossRef\]](#)

60. Firestone, R.B. Nuclear Data Sheets for $A = 186$. *Nucl. Data Sheets* **1988**, *55*, 585–664. [\[CrossRef\]](#)

61. Kondev, F.G.; Juutinen, S.; Hartley, D.J. Nuclear Data Sheets for $A = 188$. *Nucl. Data Sheets* **2018**, *150*, 1–364. [\[CrossRef\]](#)

62. Singh, B.; Chen, J. Nuclear Data Sheets for $A = 190$. *Nucl. Data Sheets* **2020**, *169*, 1–390. [\[CrossRef\]](#)

63. Baglin, C.M. Nuclear Data Sheets for $A = 192$. *Nucl. Data Sheets* **2012**, *113*, 1871–2111. [\[CrossRef\]](#)

64. Singh, B. Nuclear Data Sheets for $A = 194$. *Nucl. Data Sheets* **2006**, *107*, 1531–1746. [[CrossRef](#)]
65. Huang, X. Nuclear Data Sheets for $A = 196$. *Nucl. Data Sheets* **2007**, *108*, 1093–1286. [[CrossRef](#)]
66. Huang, X. Nuclear Data Sheets for $A = 198$. *Nucl. Data Sheets* **2009**, *110*, 2533–2688. [[CrossRef](#)]
67. Available online: <https://www.nndc.bnl.gov/ensdf/> (accessed on 1 January 2020).
68. Morinaga, H.; Yamazaki, T. *In-Beam Gamma-Ray Spectroscopy*; North Holland Publishing Company: Amsterdam, The Netherlands, 1976; Volume 54. Available online: https://inis.iaea.org/search/search.aspx?orig_q=RN:8314742 (accessed on 1 January 2020).
69. Fossan, D.B.; Herskind, B. Half-lives of first 2^+ states ($150 < A < 190$). *Nucl. Phys. A* **1963**, *40*, 24–33.